

A Mathematical Model for the Simulation of the Hemodynamics in a Patient-Specific Kidney

Fenfen Qi^[0009-0004-5343-8839], Yingzhi Liu^[0000-0001-9962-7310],
Rongliang Chen^[0000-0002-5253-0412], and Xiao-Chuan Cai^[0000-0003-0296-8640]

1 Introduction

Kidneys play a crucial role in the human body by filtering waste products and excess water from the blood to produce urine. To perform such a complex process, approximately 19% of the total cardiac output from the heart is supplied to the kidneys [11]. However, certain pathological factors such as the renal artery stenosis may lead to a reduced blood flow to certain part of the kidney, potentially compromising the kidney function. The renal arteriography, as a gold standard, is a commonly used method to assess the health of the blood vessels supplying blood to kidneys, which provides valuable information but exposes the patients to the radiation. Image-based numerical simulations of human hemodynamics have emerged as a promising alternative, enhancing our understanding of the kidney behavior for certain vascular diseases [3, 8, 1].

In this work, we present a numerical method for the simulation of blood flows in a patient-specific kidney including the renal artery, the renal vein and the kidney tissue segmented from the medical images. To mathematically model the hemodynamics of the kidney, we adopt a multiphysics approach coupling a free flow in the renal vascular region described by the three-dimensional (3D) unsteady Stokes equations with a porous medium flow in the kidney tissue modeled by the Darcy equations through three interface conditions [7]. We mention that similar coupled approaches

Fenfen Qi
Department of Mathematics, University of Macau, Macau, China, e-mail: yc27956@um.edu.mo

Yingzhi Liu
Department of Mathematics, University of Macau, Macau, China, e-mail: yingzhiliu@um.edu.mo

Rongliang Chen
Shenzhen Institutes of Advanced Technology, Chinese Academy of Sciences, Shenzhen, China,
e-mail: rl.chen@siat.ac.cn

Xiao-Chuan Cai
Department of Mathematics, University of Macau, Macau, China, e-mail: xccai@um.edu.mo

have also been applied to other organs such as the human liver [9] and myocardia [4]. To discretize the coupled system, we utilize a stabilized P1-P1-P1 finite element method on an unstructured tetrahedral mesh in space and an implicit backward Euler method in time.

As the discretized system is a large sparse saddle-point system, we further propose a Krylov subspace method accelerated by a two-level additive Schwarz preconditioner to efficiently solve it. To construct a robust coarse preconditioner, we introduce a mixed-dimensional method by combining a 1D central-line coarse preconditioner in the vascular region and a 3D coarse preconditioner in the kidney tissue region. Note that we employ different coarse basis functions for specified fields such as the conical basis functions for the velocity and the radial basis function for the pressure in the kidney. In the numerical experiments, a simulation of blood flows with patient-specific geometries and realistic parameters is carried out. The results demonstrate the effectiveness and robustness of the new preconditioner.

2 Coupled unsteady Stokes-Darcy model

In the patient-specific geometry Ω shown in Fig. 1, we consider the coupled unsteady Stokes-Darcy equations to model the blood flow in the renal artery and vein (fluid domain Ω_f) and in the kidney tissue (porous medium domain Ω_p). Specifically, the blood flows in the fluid domain Ω_f are described by the unsteady incompressible Stokes equations

$$\begin{cases} \rho \frac{\partial \mathbf{u}_f}{\partial t} - \nabla \cdot \mathbb{T}(\mathbf{u}_f, p_f) = \mathbf{f}_f, & \text{in } \Omega_f \times (0, T], \\ \nabla \cdot \mathbf{u}_f = 0, & \text{in } \Omega_f \times (0, T], \\ \mathbf{u}_f(x, 0) = \mathbf{u}_0(x), & \text{in } \Omega_f, \end{cases} \quad (1)$$

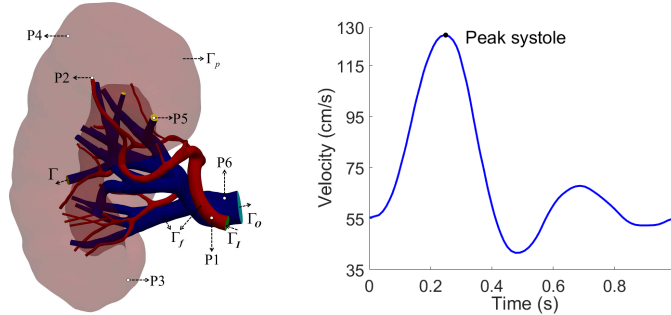


Fig. 1 A patient-specific geometry including the renal artery in red, the vein in blue and the kidney tissue in brown and a time-dependent inflow velocity profile in a cardiac cycle.

where \mathbf{u}_f and p_f are the blood velocity and the pressure in the vessels, respectively, ρ is the blood density, \mathbf{f}_f and \mathbf{u}_0 are the given source term and the initial velocity, $\mathbb{T}(\mathbf{u}_f, p_f) = -p_f\mathbb{I} + 2\mu\mathbb{D}(\mathbf{u}_f)$ is the Cauchy stress tensor, \mathbb{I} is the identity tensor, μ is the kinematic viscosity of the blood, \mathbb{D} is the the deformation tensor defined as $\mathbb{D}(\mathbf{u}_f) = 1/2(\nabla\mathbf{u}_f + \nabla\mathbf{u}_f^T)$. In the porous medium domain Ω_p , the flow is governed by the Darcy equation

$$\begin{cases} S_0 \frac{\partial p_p}{\partial t} - \nabla \cdot (\mathbb{K}\nabla p_p) = f_p, & \text{in } \Omega_p \times (0, T], \\ p_p(x, 0) = p_{p,0}(x), & \text{in } \Omega_p, \end{cases} \quad (2)$$

where p_p is the pressure in the kidney tissue, S_0 denotes the mass storativity coefficient, \mathbb{K} represents the permeability tensor assumed to be symmetric and positive definite, and $p_{p,0}$ is the given initial pressure.

Let $\Gamma = \overline{\Omega_f} \cap \overline{\Omega_p}$ denote the interface between the fluid and the porous medium. To couple the Stokes and the Darcy equation, we use the following three interface conditions on the interface Γ

$$\mathbf{u}_f \cdot \mathbf{n}_f = (\mathbb{K}\nabla p_p) \cdot \mathbf{n}_p, \quad (3)$$

$$-\mathbf{n}_f \cdot (\mathbb{T}(\mathbf{u}_f, p_f) \cdot \mathbf{n}_f) = p_p, \quad (4)$$

$$-\boldsymbol{\tau}_i \cdot (\mathbb{T}(\mathbf{u}_f, p_f) \cdot \mathbf{n}_f) = \alpha \boldsymbol{\tau}_i \cdot \mathbf{u}_f, \quad (i = 1, 2), \quad (5)$$

here \mathbf{n}_f and \mathbf{n}_p denote the unit outward normal vectors to the fluid region and the porous medium region, respectively, particularly $\mathbf{n}_f = -\mathbf{n}_p$ on the interface, $\{\boldsymbol{\tau}_i\}_{i=1}^2$ denote the unit tangential vectors to the interface and α is a parameter in the BJS condition (5).

On the boundaries, we impose a Dirichlet velocity profile in a cardiac cycle [10] shown in Fig. 1 on the inlet Γ_I , a constant pressure condition on the outlet Γ_O , the no-slip condition on the vascular wall $\Gamma_f = \partial\Omega_f \setminus (\Gamma \cup \Gamma_I \cup \Gamma_O)$, and the pressure condition on the wall of the kidney tissue $\Gamma_p = \partial\Omega_p \setminus \Gamma$. More precisely, these conditions are written as

$$\begin{aligned} \mathbf{u}_f &= \mathbf{u}_I, & \text{on } \Gamma_I \times (0, T], \\ \mathbf{u}_f &= \mathbf{0}, & \text{on } \Gamma_f \times (0, T], \\ -\mathbb{T}(\mathbf{u}_f, p_f) \cdot \mathbf{n}_f &= p_O \cdot \mathbf{n}_f, & \text{on } \Gamma_O \times (0, T], \\ -\mathbb{K}\nabla p_p \cdot \mathbf{n}_p &= 0, & \text{on } \Gamma_p \times (0, T], \end{aligned} \quad (6)$$

where \mathbf{u}_I is the inlet velocity and p_O is the outlet pressure. Then the weak formulation of (1)–(6) is to find $\mathbf{u}_f \in \mathbf{V}_f$, $p_f \in W_f$, $p_p \in W_p$, such that

$$\begin{aligned} & \left(\rho \frac{\partial \mathbf{u}_f}{\partial t}, \mathbf{v}_f \right)_{\Omega_f} + \left(S_0 \frac{\partial p_p}{\partial t}, q_p \right)_{\Omega_p} + (2\mu\mathbb{D}(\mathbf{u}_f), \mathbb{D}(\mathbf{v}_f))_{\Omega_f} + \alpha \sum_{i=1}^2 (\boldsymbol{\tau}_i \cdot \mathbf{u}_f, \boldsymbol{\tau}_i \cdot \mathbf{v}_f)_{\Gamma} \\ & - (p_f, \nabla \cdot \mathbf{v}_f)_{\Omega_f} + (q_f, \nabla \cdot \mathbf{u}_f)_{\Omega_f} + (\mathbb{K}\nabla p_p, \nabla q_p)_{\Omega_p} + (p_p, \mathbf{v}_f \cdot \mathbf{n}_f)_{\Gamma} \\ & - (\mathbf{u}_f \cdot \mathbf{n}_f, q_p)_{\Gamma} = (\mathbf{f}_f, \mathbf{v}_f)_{\Omega_f} + (f_p, q_p)_{\Omega_p} - (p_O, \mathbf{v}_f \cdot \mathbf{n}_f)_{\Gamma_O}, \end{aligned} \quad (7)$$

for all $\mathbf{v}_f \in \mathbf{V}_f^0$, $q_f \in W_f$, $q_p \in W_p$ and $t \in (0, T]$, where $(u, v)_D = \int_D uv$ is the inner product and the Sobolev spaces \mathbf{V}_f , \mathbf{V}_f^0 , W_f are given in [5] and $W_p = H^1(\Omega_p)$. We cover the computational domain Ω with an unstructured tetrahedral mesh \mathcal{T}_h consisting of the mesh \mathcal{T}_h^f in Ω_f and \mathcal{T}_h^p in Ω_p , which are matched on the interface; see Fig. 2. Then we use a stabilized P1-P1-P1 finite element method for the spatial discretization and the backward Euler method for the temporal discretization.

3 Two-level additive Schwarz preconditioner

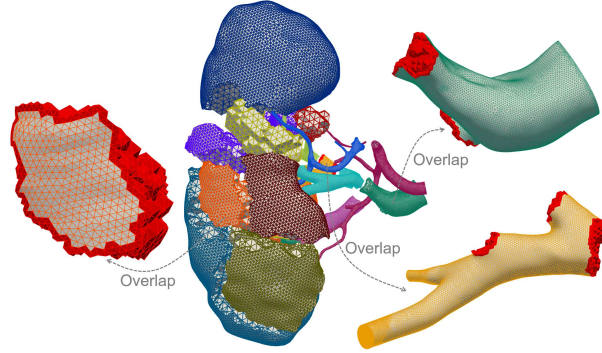


Fig. 2 A sample domain decomposition of the kidney into 10 overlapping subdomains represented by different colors and the overlapping elements are marked in red. There is no element-wise overlap between the arterial region, the venous region and the tissue region, but they share the same mesh points on the interfaces between the regions.

To solve the resulting large linear systems, we design a two-level additive Schwarz preconditioner to accelerate the convergence of a Krylov subspace method. We first divide the domain Ω into np nonoverlapping subdomains Ω_i^0 , $i = 1, \dots, np$, see Fig. 2, and then extend them into overlapping subdomains Ω_i by including δ layers of elements from the neighboring subdomains. We remark that there is no element-wise overlap between the arterial region, the venous region and the tissue region, but they share the same mesh points on the interfaces between the regions. When constructing the subdomain matrices, the interface values appear in all subdomains sharing the same mesh points. The two-level Schwarz preconditioner M_{2s}^{-1} takes the form

$$M_{2s}^{-1} = \sum_{i=1}^{np} (R_i^0)^T A_i^{-1} R_i + E_c A_c^{-1} R_c := M_{1s}^{-1} + M_c^{-1}, \quad (8)$$

where $A_i = R_i A R_i^T$ is the local matrix restricted in the i th subdomain, M_{1s}^{-1} is the one-level preconditioner [2] and M_c^{-1} is a coarse preconditioner. Here R_i (R_i^0)

denotes the natural restriction matrix corresponding to the subdomain Ω_i (Ω_i^0). R_c and E_c are the coarse restriction and extension matrices whose construction is crucial to determine the performance of the coarse preconditioner. The coarse matrix A_c can be obtained by $A_c = R_c A E_c$. Following the idea of the mixed-dimensional coarse preconditioner in blood flow problems [6], we introduce a 1D-3D coarse preconditioner consisting of a 1D central-line coarse preconditioner in the vascular region and a 3D coarse preconditioner in the kidney region.

To construct the coarse space, different coarse basis functions are used for different fields. Specifically, in the vascular region Ω_f , we extract the centerline Ω_f^{cl} parameterized by the arc length s and then partition it to generate a coarse mesh with mesh points $\{x_{cl}^i\}_{i=1}^{N_{cl}}$. For each mesh point x_{cl}^i , we define \mathcal{I}_i as the collection of its adjacent points and D_i as its influence region which is enclosed by the wall and the cross sections C_s^j , $j \in \mathcal{I}_i$. For the velocity, we define the coarse conical basis function

$$\varphi_{cl}^i(s, r, \theta) = \zeta \left(\frac{r(s)}{r_{\theta}(s)} \right) \phi_{cl}^i(s) \tau_{cl}^i, \quad (s, r, \theta) \in D_i, \quad (9)$$

for each mesh points x_{cl}^i , where the pair (r, θ) is the polar coordinates in C_s^i , $r_{\theta}(s)$ is the radial radius, τ_{cl}^i is the unit tangential vector along the centerline at x_{cl}^i , and ζ is a radial profile function

$$\zeta(y) = (1 - y^\gamma), \quad y \in [0, 1], \quad (10)$$

with the profile parameter γ , and ϕ_{cl}^i is a linear Lagrangian basis function defined on the centerline, satisfying

$$\phi_{cl}^i(s(x_{cl}^j)) = \delta_{ij}, \quad \forall i, j = 1, \dots, N_{cl}, \quad (11)$$

δ_{ij} being the Kronecker delta. For the pressure we directly use ϕ_{cl}^i as the coarse basis function.

For the kidney tissue region, we define the coarse basis functions $\{\varphi_c^i\}_{i=1}^{N_c}$ by the Wendland radial basis function [12]

$$\varphi_c^i(x; \xi) = \begin{cases} \left(1 - \frac{|x-x_c^i|}{\xi}\right)^4 \left(1 + \frac{4|x-x_c^i|}{\xi}\right), & |x-x_c^i| \leq \xi; \\ 0, & \text{otherwise,} \end{cases} \quad (12)$$

where $\{x_c^i\}_{i=1}^{N_c}$ indicates the coarse mesh points and ξ is the shape parameter.

Remark 1 For the comparison in the experiments, we also consider a 0D coarse preconditioner [5] where the coarse basis functions are the characteristic functions in the nonoverlapping subdomains for both Ω_f and Ω_p

$$\varphi_i(x) = \begin{cases} 1, & x \in \Omega_i^0, \\ 0, & \text{otherwise,} \end{cases} \quad (13)$$

and a 1D-0D coarse preconditioner where the coarse basis functions are the same as the proposed 1D-3D coarse preconditioner in the vascular region Ω_f but are replaced by the characteristic functions (13) in the kidney tissue region Ω_p .

4 Numerical experiments

In this section, some numerical experiments are presented to simulate the blood flows in a patient-specific kidney, and also to study the performance of the proposed preconditioner. In all experiments, the permeability is assumed to be isotropic and homogeneous, i.e., $\mathbb{K} = k\mathbb{I}$, where k is a scalar permeability set to be $k = 4 \times 10^{-5} \text{ cm}^3 \cdot \text{s/g}$ and the storativity $S_0 = 10^{-8} \text{ cm} \cdot \text{s}^2/\text{g}$. The discretized system is solved by a right-preconditioned restarted GMRES(100) method and the iteration is stopped when the residual reaches the relative tolerance 10^{-9} or the absolute tolerance 10^{-6} . The maximum number of iterations is set to be 600. To investigate the performance of the proposed preconditioner, we compare the number of iterations for four preconditioners including the one-level additive Schwarz preconditioner M_{1s}^{-1} and the two-level additive Schwarz preconditioners M_{2s}^{-1} with the 0D, 1D-0D and 1D-3D coarse preconditioners. For these four preconditioners, the LU and incomplete LU (ILU) factorizations are used as the coarse solver and subdomain solvers, respectively. We use an unstructured mesh with 488,047 mesh points and the time step size $\Delta t = 0.01$ for the discretization. In Table 1, np and δ denote the number of subdomains and the overlapping layers, respectively.

In Fig. 3, we show the distributions of the pressure in the artery, the vein and the kidney tissue at the peak systole ($t = 0.24 \text{ s}$). We can observe that the artery exhibits significantly higher pressures, while the pressure in the vein remains relatively constant. Furthermore, we also see an obvious change of the pressure in the kidney tissue, especially near the interface. In Fig. 4, the waveforms of pressure in a cardiac cycle indicate that the pressures in the artery (P1 and P2) and the kidney (P3 and P4) are pulsatile but remain almost unchanged in the vein (P5 and P6).

Further, we investigate the impact of the ILU fill-in level and the overlapping size on the performance of the proposed algorithm in Table 1. We can see that among all preconditioners, the new 1D-3D coarse preconditioner with ILU(2) offers the best performance in terms of the number of iterations. For a fixed ILU fill-in level, the number of iterations almost decreases as the overlapping size δ increases from 0 to 2. Fig. 5 plots the iteration and the residual histories for different preconditioners. It shows that the two-level preconditioner significantly improves the convergence of the one-level preconditioner and the proposed preconditioner has the best performance.

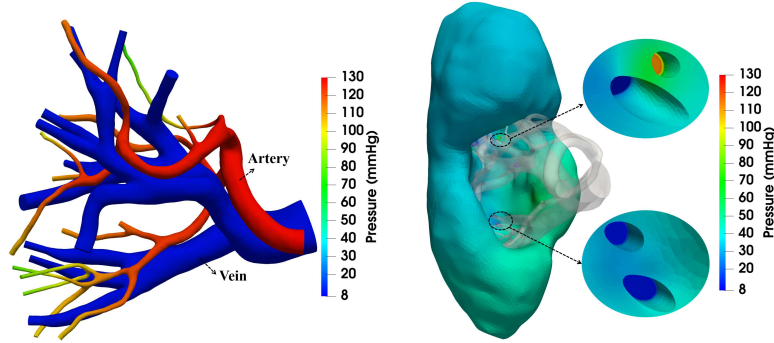


Fig. 3 Distributions of the pressure in the vascular region (left) and the kidney tissue (right) at the peak systole.

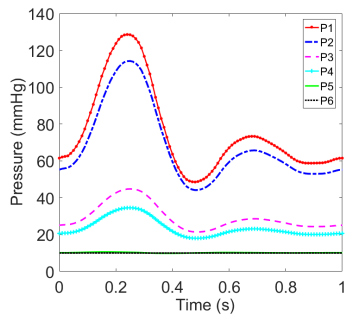


Fig. 4 The temporal changes of the pressure in a cardiac cycle at six monitoring points.

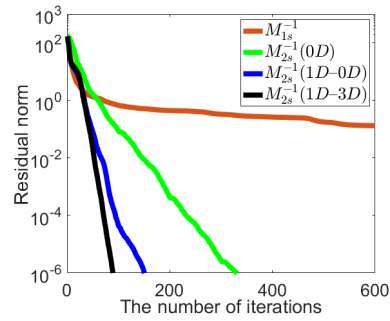


Fig. 5 The iteration and the residual histories for four different preconditioners.

Table 1 Performances of different Schwarz preconditioners in terms of the number of iterations.

Mesh	np	ILU	δ	One-level	Two-level		
					0D	1D-0D	1D-3D
488,047	256			0	-	338	217
				1	-	308	281
				2	-	292	282
				0	-	350	81
				2	1	230	76
				2	-	290	114

5 Conclusions

In this paper, we present a mathematical model for the simulation of blood flows in the patient-specific renal artery, the vein and the kidney tissue, the model is constructed by coupling the 3D unsteady Stokes equations for the renal vessels and Darcy equations for the kidney tissue. To numerically solve the coupled system, a

stabilized P1-P1-P1 finite element method and an implicit backward Euler method are used. With the purpose of the acceleration, we propose a novel two-level additive Schwarz preconditioner with a mixed-dimensional coarse preconditioner incorporating a 1D central-line coarse preconditioner in the vascular region and a coarse mesh preconditioner in the tissue region. The numerical results show that the proposed preconditioner has a good performance for the complex patient-specific kidney.

Acknowledgements This work was supported by the NSFC through Grant 12201658 and the FDCT through Grant 0141/2021/A3, 0079/2021/AFJ.

References

1. Bortolussi, C.: Computational modeling of flow in the kidney (2018)
2. Cai, X.C., Sarkis, M.: A restricted additive Schwarz preconditioner for general sparse linear systems. *SIAM J. Sci. Comput.* **21**(2), 792–797 (1999)
3. Chen, R., Wu, B., Cheng, Z., Shiu, W.S., Liu, J., Liu, L., Wang, Y., Wang, X., Cai, X.C.: A parallel non-nested two-level domain decomposition method for simulating blood flows in cerebral artery of stroke patient. *Int. J. Numer. Methods Biomed. Eng.* **36**(11), e3392 (2020)
4. Di Gregorio, S., Fedele, M., Pontone, G., Corno, A.F., Zunino, P., Vergara, C., Quarteroni, A.: A computational model applied to myocardial perfusion in the human heart: from large coronaries to microvasculature. *J. Comput. Phys.* **424**, 109836 (2021)
5. Liu, Y., Cai, X.C.: Two-level additive Schwarz methods for three-dimensional unsteady Stokes flows in patient-specific arteries with parameterized one-dimensional central-line coarse preconditioner. *J. Comput. Phys.* **490**, 112290 (2023)
6. Liu, Y., Qi, F., Cai, X.C.: An aneurysm-specific preconditioning technique for the acceleration of Newton-Krylov method with application in the simulation of blood flows. *Int. J. Numer. Methods Biomed. Eng.* **39**(12), e3771 (2023)
7. Mikelic, A., Jäger, W.: On the interface boundary condition of Beavers, Joseph, and Saffman. *SIAM J. Appl. Math.* **60**(4), 1111–1127 (2000)
8. Quarteroni, A., Manzoni, A., Vergara, C.: The cardiovascular system: mathematical modelling, numerical algorithms and clinical applications. *Acta Numer.* **26**, 365–590 (2017)
9. Stoter, S.K., Müller, P., Cicalese, L., Tuveri, M., Schillinger, D., Hughes, T.J.: A diffuse interface method for the Navier–Stokes/Darcy equations: Perfusion profile for a patient-specific human liver based on MRI scans. *Comput. Methods Appl. Mech. Engrg.* **321**, 70–102 (2017)
10. Taylor, C.A., Hughes, T.J., Zarins, C.K.: Finite element modeling of three-dimensional pulsatile flow in the abdominal aorta: relevance to atherosclerosis. *Ann. Biomed. Eng.* **26**, 975–987 (1998)
11. Valentin, J.: Basic anatomical and physiological data for use in radiological protection: reference values. *Ann. ICRP* **32**(3–4), 1–277 (2002)
12. Wendland, H.: Piecewise polynomial, positive definite and compactly supported radial functions of minimal degree. *Adv. Comput. Math.* **4**, 389–396 (1995)